RETINAL IMAGE FUSION AND REGISTRATION

L. Kubecka*, J. Jan*
* Brno University of Technology/Department of Biomedical Engineering, Kolejni 4, Brno, Czech Republic

Email Address: libor@kubecka.info

Abstract: The contribution deals with the processing of the 2D multi-spectral images, especially their fusion, using an orthogonal discrete wavelet representation of previously registered image pairs. The method is based on decomposition of gradient of the vector image by computation of eigen-values of the first differential of the vector image. An application of the method to multimodal ophthalmic images is presented. Two multimodal images (color fundus photograph and Heilderberg retina tomography image) are preprocessed and registered by the originally designed registration method based on maximization of the modified mutual information as the global similarity criterion. Controlled random search is used as the robust optimizer. 98% of images in the testing set containing 336 images have been successfully registered according to the subjective evaluation of the human observer. Further, results of the image fusion are presented as well as the first evaluation of segmentation of the optic nerve head contour.

Introduction

As a result of rapid development of new imaging modalities, the demand for simultaneous processing of several of these images has been arisen in past few decades. Especially the area of medical imaging often produces many types of images of the same scene e.g. MRI images taken with various parameters (T1, T2, …), CT and PET images, images enhanced by contrast agents. Another type of multi-spectral images is provided by remote-sensing or infrared imaging. Nowadays, processing of these multi-spectral images is usually done by component-by-component processing, but this approach has several disadvantages as if the inter-component dependencies are not taken into account. For this reason, the fusion can be done to obtain scalar image and then usual processing can be performed or processing of the image is carried out by generalized vector methods. In [1] it is shown that principle component analysis (PCA) is a relevant method for merging remotely sensed imagery because of its ability to reduce the dimensionality of the original data from n to 2 or 3 by finding principal component, which contain majority of information. In [2] the wavelet-transform-based image fusion is presented, where to-be-fused images are first decomposed using discrete wavelet transform (DWT), then a fusion decision map is generated based on a set of fusion rules and the fused wavelet coefficient map is constructed from the wavelet coefficients of the source images according to the fusion decision map. Finally the fused image is obtained by performing the inverse wavelet transform. The method for merging high-resolution panchromatic image (SPOT) and a low-resolution multi-spectral image (LANDSAT) presented in [3] consists of adding the wavelet coefficients of the high-resolution image to the multi-spectral image data. The method is compared to standard intensity-hue-saturation (IHS) method. The algorithm using the orthogonal gradient representation of multi-spectral images and its applications in image merging and color image demosaicing is described in [4]. In this paper, we present this slightly modified method for automatic fusion of images acquired from two imaging modalities, namely of the confocal scanning laser ophtalmoscope (CSLO) image and color photographic image of the retina, sometimes called fundus photographs (CFP).

Prior to fusion, both images are registered using the originally designed algorithm based on robust maximization of the mutual information similarity criterion. The fusion is done with expectation of benefits to consequential segmentation of the optic disk in the fused vector valued image data. This segmentation is a necessary pre-step for evaluating retinal images and also for better diagnosing of glaucoma and cerebro-vascular diseases. Nowadays, this segmentation is performed by medical experts but there are two serious problems. The first problem is the inter- and intra-operator variability reported by many studies (e.g. [5]), the second one is unsatisfactory sensitivity and specificity of individual diagnostic methods [6], [7], and finally the process of diagnosis is slow and the costs are high.

For this reason the automatic segmentation is necessary especially for glaucoma screening where large amount of people should be examined.

Materials and Methods

The process of diagnosis of multi-spectral retinal image data can be split into several stand-alone phases. First, both images have to be preprocessed. In the second step both images are registered into one vector-valued image. Thirdly the fusion of the vector valued image is performed. Then the optic disc and vessels are segmented and the shape parameters of segmented structures are computed [8]. Finally images are

ISSN: 1727-1983

classified according to these parameters. Only the first four steps are presented in this paper.

Due to reflectance characteristics of the retina the maximum amount of information is contained in the green and blue channel. For the purpose of consequent registration, the principle component analysis (PCA) [9] is done and only the band belonging to the highest eigen-value is used for the subsequent processing. Both images are corrupted by non-homogenous illumination; therefore its correction is necessary [10]. Unfortunately, this procedure significantly emphasizes noise; hence edge preserving smoothing is done making use of anisotropic diffusion [11].

Since both images are generally not in the same coordinate system, image registration has to be performed. The registration is defined as searching for the best geometric transform describing the relationship between the reference and the registered images. The used affine transform T is supposed to depend on a vector parameter α, encompassing shift, rotation, scale and shear. The vector parameter is found by optimization,

$$\alpha_0 = \arg \max_{\alpha} \left[C\left(\mathrm{F}, \mathrm{M}\left(T_\alpha\right)\right)\right], \qquad (1)$$

where **F** is the reference image, **M** is the registered image, which is spatially transformed by T_α to the coordinates of the reference image. The registration quality, corresponding to the transform T is evaluated by the criterial function C. $T_{\alpha 0}$ is then the optimal transform with respect to the criterion. As was proven in [12], affine transform provides sufficient flexibility for restoration of misregistration between both images. Modified mutual information was used as the similarity criterion since it is able to cope with substantially differing contrast mechanisms of the corresponding features in the images. Mutual information of two images is defined as follows:

$$\mathrm{MI}(T,\mathrm{F},\mathrm{M}) = \sum_{x \in F} p_{FM}[\mathrm{F}(\mathbf{x}),\mathrm{M}(T(\mathbf{x}))] \log \frac{p_{FM}[\mathrm{F}(\mathbf{x}),\mathrm{M}(T(\mathbf{x}))]}{p_F[\mathrm{F}(\mathbf{x})]p_M[\mathrm{M}(T(\mathbf{x}))]},$$

where x is spatial position in reference image coordinate system, F is fixed reference image, M is moving image, both images are considered random variables therefore p_F [F(x)] and p_M [M(T(x))] denotes probability of occurrence of brightness value corresponding to current position in images F and M and p_{FM}[F(x),M(T(x))] denotes mutual probability. All these probabilities can be evaluated from mutual histogram which is constructed as follows:

$$h(\mathrm{F}(\mathbf{x}),\mathrm{M}(T(\mathbf{x}))) = h(\mathrm{F}(\mathbf{x}),\mathrm{M}(T(\mathbf{x}))) + 1, \text{for all } \mathbf{x} \in \mathrm{F} \quad (2)$$

where h is usually symmetric 2D matrix of size *Nbins* and the value $h(a,b)$, $a \in [0, Nbins-1]$, $b \in [0, Nbins-1]$ is equal to the number of corresponding pairs having intensity value in the range $[a \cdot sbF, (a+1) \cdot sbF]$ in the first image and intensity value $[b \cdot sbM, (b+1) \cdot sbM]$ in the second image, where *Nbins* is number of bins for histogram calculation. Size of intensity bin *sbF* and *sbM* are defined as follows:

$$sbF = \frac{\max_{x,y}(F(x,y)) - \min_{x,y}(F(x,y))}{Nbins}, \quad sbM = \frac{\max_{x,y}(M(x,y)) - \min_{x,y}(M(x,y))}{Nbins} \qquad (3)$$

Two commonly used algorithms to estimate the joint histogram of two images are intensity interpolation and partial volume interpolation performed directly in joint histogram [13]. However, when the two images have the same spatial resolution along at least one direction, both algorithms may suffer from interpolation-induced artifacts [14]. The reason is that, under this condition, the number of grid-aligned pixels may change discontinuously when the displacement involved in the geometrical transformation along that direction changes. To avoid the formation of the artifact patterns we have used nearest neighbor interpolation and 25 bins for creating mutual histogram. The computation of probabilities is then done using new smoothed mutual histogram *smH* acquired by convolving an original mutual histogram with a smoothing linear convolution filter with kernel k and size 3x3, thus the probabilities can be evaluated as:

$$p_{FM}[\mathrm{F}(\mathbf{x}),\mathrm{M}(T(\mathbf{x}))] = \frac{h[\mathrm{F}(\mathbf{x}),\mathrm{M}(T(\mathbf{x}))]}{\sum_{\mathrm{F}(\mathbf{x}),\mathrm{M}(T(\mathbf{x}))} h[\mathrm{F}(\mathbf{x}),\mathrm{M}(T(\mathbf{x}))]}$$

$$p_F[\mathrm{F}(\mathbf{x})] = \sum_{\mathrm{F}(T(\mathbf{x}))} p_{FM}[\mathrm{F}(\mathbf{x}),\mathrm{M}(T(\mathbf{x}))] \qquad (4)$$

$$p_M[\mathrm{M}(T(\mathbf{x}))] = \sum_{\mathrm{F}(\mathbf{x})} p_{FM}[\mathrm{F}(\mathbf{x}),\mathrm{M}(T(\mathbf{x}))]$$

The final metric value can be evaluated as follows:

$$\mathrm{I}(T,\mathrm{F},\mathrm{M}) = \mathrm{MI}(T,\mathrm{F},\mathrm{M}) \cdot \frac{nM}{nF}, \qquad (5)$$

where nF is total number of pixels in fixed image and nM is number of corresponding pixels transformed inside moving image, thus the non-overlapping area is penalized. Despite all these modifications the shape of the criterion function still can not be approximated by quadratic form and consequently a more robust optimization algorithm has to be used. In was shown that controlled random search is robust enough. The registration can be described as follows in the flow diagram on the Figure 1. Optimizer selects transformation parameters, then every point of the moving image is transformed and if it is lying in the area of the fixed image, it is involved into similarity measure calculation. When fitness value is calculated, optimizer derives next transform parameters from this value or possibly from values visited so far and the whole cycle repeats until the termination condition is fulfilled.

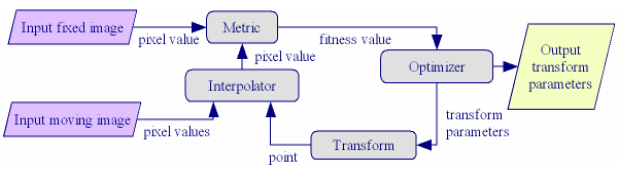

Figure 1: Image registration schema.

ISSN: 1727-1983

After proper registration a new vector-valued image is obtained and subsequent processing can be done in two ways. Either the vector-valued image can be processed directly using vector image processing techniques or the fusion of the vector-valued image into a scalar-valued image can be performed with benefits of following standard scalar image processing.

Image fusion is defined as creating a single image from a set of input images. The fused image should have more complete information which is more useful for human or machine perception. Image fusion can improve reliability (by redundant information) and capability (by complementary information) of subsequent processing.

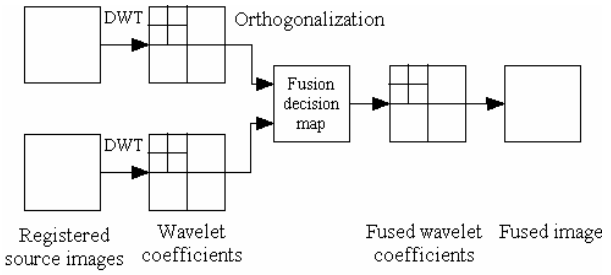

Figure 2: Illustration of image fusion making use of wavelet transform

The image fusion can be done making use of discrete wavelet decomposition, where images are fused by merging their wavelet coefficients. This merging can be based on creating sc. fusion decision map [2] or the wavelet representation for multi-valued images is made by combining detail (edge) information contained in vector-image bands into one set of details using DiZenzo's first fundamental form [4]. It means that subsequent processing of the scalar image will utilize the advantage of processing all the vector image bands simultaneously. This algorithm is exploited and described in this paper. For obtaining the image in the image domain inverse wavelet transform is applied. Following a development, similar to [4], we obtain:

Let $\mathbf{I}(x,y)$ be a vector valued image with components $I_n(x,y)$, $n = 1, \ldots, N$ and let $\mathbf{L}$ is a vector operator whose components are both linear operators L_x, L_y defined as isotropic convolution operators applied in direction x or y. Examples of such a operator can be gradient operator $\nabla = (\partial/\partial x, \partial/\partial y)$, Gaussian gradient filter. Two proposal of the vector operator $\mathbf{L}$ have been done:

$$\mathbf{L}(\mathbf{I}) = \frac{1}{N}\sum_n \mathbf{L}(I_n) \quad \text{or}$$

$$\mathbf{L}(\mathbf{I}) = L(I_j),\ j = \max_n \|\mathbf{L}(I_n)\|^2$$

However, both procedures do not take the bands into account simultaneously, hence there is a problem with averaging opposite vectors, which could annihilate despite that they should have some information. For that reason multi-valued 'maximal length' and 'direction of maximal length' were defined making use of quadratic form of the image differential [4]. The differential of $d\mathbf{I}$ in Euclidean space can be described as:

$$d\mathbf{I} = \frac{\partial \mathbf{I}}{\partial x}dx + \frac{\partial \mathbf{I}}{\partial y}dy$$

And its squared norm is given by (sums are over all components of the vector image):

$$(d\mathbf{I})^2 = \|\mathbf{I}_x\|^2 dx^2 + 2\mathbf{I}_x\mathbf{I}_y dx dy + \|\mathbf{I}_y\|^2 dy^2 = \begin{pmatrix} dx \\ dy \end{pmatrix}^T \cdot \begin{pmatrix} \left\|\frac{\partial \mathbf{I}}{\partial x}\right\|^2 & \frac{\partial \mathbf{I}}{\partial x}\cdot\frac{\partial \mathbf{I}}{\partial y} \\ \frac{\partial \mathbf{I}}{\partial y}\cdot\frac{\partial \mathbf{I}}{\partial x} & \left\|\frac{\partial \mathbf{I}}{\partial y}\right\|^2 \end{pmatrix} \cdot \begin{pmatrix} dx \\ dy \end{pmatrix}$$

And for the norm of the differential of scalar product $\mathbf{L}(\mathbf{I})\cdot d\mathbf{x} = L_x(\mathbf{I})dx + L_y(\mathbf{I})dy$ can be written:

$$(\mathbf{L}(\mathbf{I})\cdot d\mathbf{x})^2 = \begin{pmatrix} dx \\ dy \end{pmatrix}^T \cdot \begin{pmatrix} \sum (L_x(I_n))^2 & \sum (L_x(I_n))(L_y(I_n)) \\ \sum (L_y(I_n))(L_x(I_n)) & \sum (L_y(I_n))^2 \end{pmatrix} \cdot \begin{pmatrix} dx \\ dy \end{pmatrix} = \begin{pmatrix} dx \\ dy \end{pmatrix}^T \cdot \begin{pmatrix} G_{xx} & G_{xy} \\ G_{yx} & G_{yy} \end{pmatrix} \cdot \begin{pmatrix} dx \\ dy \end{pmatrix} = d\mathbf{x}^T \cdot G \cdot d\mathbf{x} \qquad (6)$$

The matrix G is symmetric and semi positive-definite hence its eigen-values are real and non-negative. The quadratic form (6) represents changes in vector-valued image. The direction of maximal change is defined by the eigenvector θ^1 of the matrix $\mathbf{G}$ corresponding to the maximal eigen-value λ^1 representing the maximal squared length of the vector $\mathbf{L}(\mathbf{I})$ whereas the second eigenvector lies in the orthogonal direction of maximal length and the corresponding eigen-value denotes minimal variations of the matrix. Consistence of this theory for a scalar valued image (N=1) is obvious, the largest eigen-value is $\lambda^1 = \|\nabla I\|^2$ and the corresponding eigenvector $\theta^1 = \frac{\nabla I}{\|\nabla I\|}$, we can also see that $\nabla I = \sqrt{\lambda^1}\cdot\theta^1$. The other eigen-value equals zero, for multi-valued image this eigen-value is generally different from zero. These eigen-values are indeed well adapted to discriminate different geometric cases:

If $\lambda^1 \cong \lambda^2 \cong 0$, there are very few vector variations around the current point x, the region is almost flat and doesn't contain any edges or corners.

If $\lambda^1 >> \lambda^2$, there are a lot of vector variations. The current point may be located on a vector edge.

If $\lambda^1 \cong \lambda^2 > 0$, the current point lies on a saddle point of the vector surface, which can possibly be a vector corner.

For the purpose of fusing images it can be defined:

$$\mathbf{L}(\mathbf{I}(x,y)) \equiv \begin{pmatrix} \sqrt{\lambda^1}\theta_x^1(x,y) \\ \sqrt{\lambda^1}\theta_y^1(x,y) \end{pmatrix} \qquad (7)$$

For the fusion of the vector-valued image we used method based on discrete orthogonal wavelet decomposition [4]

By this transform, an image $f(x,y)$ is decomposed at different scales j into a lower resolution image $A_2^j f$ (sc. approximation) and three detail images $D_2^{j\,1} f$, $D_2^{j\,2} f$, $D_2^{j\,3} f$. This is done by uniform down-sampling of 2D

ISSN: 1727-1983

convolution products. At each scale $j \in [-1, J]$, $(n,m) \in Z^2$ we can write:

$$\begin{aligned} A_{2^j} f &= f(x,y) * \phi_{2^j}(-x)\phi_{2^j}(-y)\left(2^{-j}n, 2^{-j}m\right) \\ D^1_{2^j} f &= f(x,y) * \phi_{2^j}(-x)\psi_{2^j}(-y)\left(2^{-j}n, 2^{-j}m\right) \\ D^2_{2^j} f &= f(x,y) * \psi_{2^j}(-x)\phi_{2^j}(-y)\left(2^{-j}n, 2^{-j}m\right) \\ D^3_{2^j} f &= f(x,y) * \psi_{2^j}(-x)\psi_{2^j}(-y)\left(2^{-j}n, 2^{-j}m\right) \end{aligned} \quad , \quad (8)$$

Where ϕ and ψ are separable low and high bandpass filters. This wavelet transform can be computed by gradual applying 1D quadrature mirror filters Lo_D (lowpass) and Hi_D (highpass) for decomposition and symmetric filters Lo_R, Hi_R for reconstruction [4]. Let **L** be a linear convolution vector operator:

$$\mathbf{L} = \begin{pmatrix} Hi\_D_x \\ Hi\_D_y \end{pmatrix} * \quad (9)$$

Vector image **I** is then decomposed into wavelet coefficients according to the schema in the table 1.

Table 1: The whole algorithm for the multi-valued image wavelet representation.

for j^{th} scale
  for i^{th} band
    Compute i[th] approximation $A^i_{2^j}(x,y)$ (see (8)).
    Compute images $D^1_{2^j} I_i, D^2_{2^j} I_i$ by bandpass filtering using filters Lo_D_x and Lo_D_y:
    $\begin{pmatrix} D^1_{2^j} I_i \\ D^2_{2^j} I_i \end{pmatrix} = \begin{pmatrix} L^x_{2^{j+1}} A_{2^{j+1}} I_i \\ L^x_{2^{j+1}} A_{2^{j+1}} I_i \end{pmatrix}$
  end of i^{th} band
  Compute variation matrix **G** using $D^1_{2^j}\mathbf{I}, D^2_{2^j}\mathbf{I}$ (see (6))
  Diagonalize matrix G and compute fused details $D^{1+}_{2^j}(x,y), D^{2+}_{2^j}(x,y)$ using maximal eigenvalue and its eigenvector (7),
  Carry out correction of the direction using averaged details.
  Perform down sampling and filtration to compute final details $D^1_{2^j}\mathbf{I}, D^2_{2^j}\mathbf{I}, D^3_{2^j}\mathbf{I}$.
end j^{th} scale
After decomposition, following set of images is generated for each scale:
$\left\{D^{1+}_{2^j}(x,y), D^{2+}_{2^j}(x,y), D^{3+}_{2^j}(x,y)\right\}_{-1 \geq j \leq J}$ - image details.
$A^+_{2^j}(x,y)$ - the lowest resolution image.
Finally, complete wavelet reconstruction

Detail images on each scale level are computed by filtering relevant approximations using Hi_D filter, then the orthogonalization (6) is done and a new gradient representation is obtained using (7), then final down-sampling and filtering is performed defining fused detail images at current scale level. The approximation can be computed as averages of each band approximations. It can be formalized as:

$$A^+_{2^j}(x,y) = \frac{\sum_{i=1}^{N} A^i_{2^j}(x,y)}{N} \quad (10)$$

There is a problem with diagonalization caused by not uniquely specified signs of the eigenvectors. An extensive study and solution of this problem is given in [4], where the direction of maximal length is compared to the average direction, obtained by applying gradient operator on all bands separately and if directions of these vectors are different, the maximal length direction is flipped into average direction.

Due to problems with annihilation of opposite bands while averaging, we have modified this approach. We compare the direction of maximal length with the direction of the gradient of the principle component acquired from the PCA analysis of approximations of each band at the current position. For this case the scalar product of these two vectors is evaluated and the direction of the eigenvectors is maintained if the product is positive, else the eigenvectors with the opposite direction are applied in subsequent computations.

Results

The method was tested on images acquired from confocal scanning laser ophthalmoscope (CSLO), concretely we have been using the Heildeberg Retina Tomograph II (HRT). The CSLO provides three dimensional data of optic nerve head produced by focusing into different focal planes making use of confocal principle [16]. The standard color fundus camera Kowa was another modality providing color photographs of larger area of the retina than CSLO. The aim of the project is to segment correctly the optic nerve head margin [8] as needed in diagnosing glaucoma especially for screening and preventing the inter-observer variability. We have used the non-rigid affine registration for compensation of distortions between both images. Modified mutual information (5) was used as suitable similarity criterion. The controlled random search (CRS) algorithm was selected as the robust enough optimizer. The success-rate of the registration was evaluated on the set containing 334 images. First, 10% of these images were taken as training set and the parameters of the algorithm were set. Then the algorithm was tested on the other 90% of images. In that case, the success rate of the registration was only approximately 80%. This was caused by the wrong choice of the parameter space bounds, which were set to ± 3 times dispersion each of six final parameters obtained from successfully registered training set. It can be said that the training image set was not representative enough. When the falsely registered images were registered again with wider boundaries and the algorithm parameters were set to boundaries obtained by this re-registration, the rate of successfully registered images increased significantly to 98%. Another study concerning this registration algorithm in greater detail is [12].

ISSN: 1727-1983

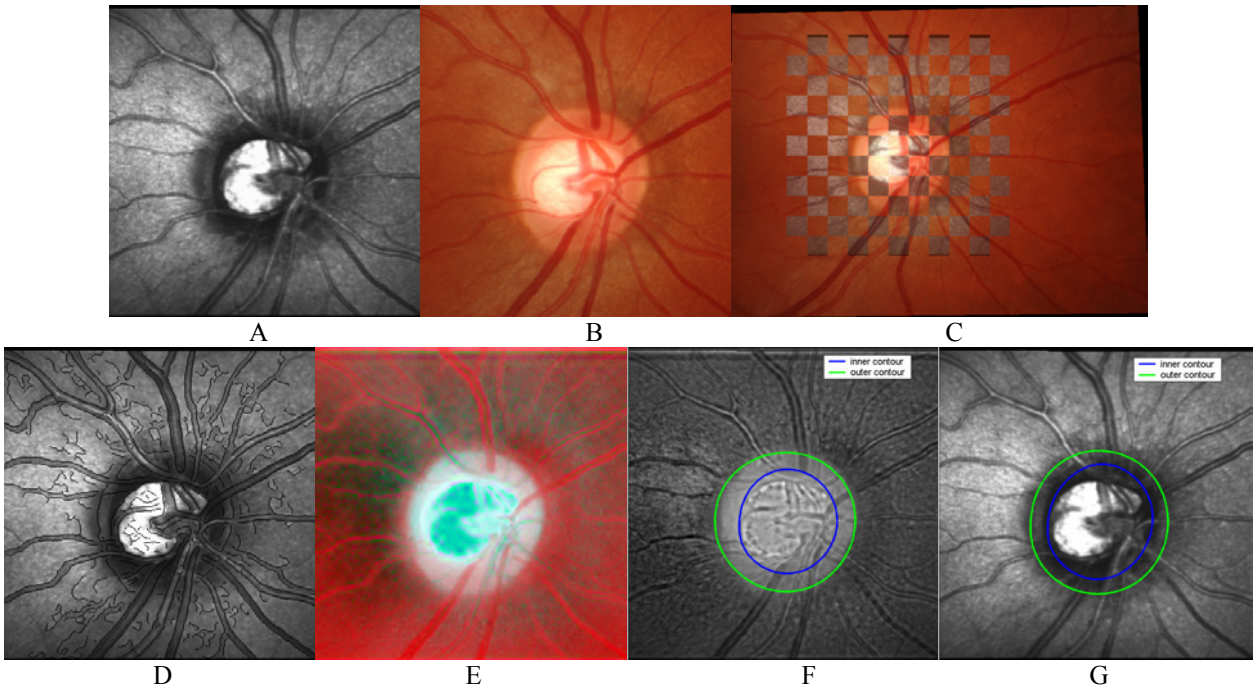

Figure 3: A - original HRT image, B – registered CFP image, C – registered CFP image with inserted mosaic of HRT image, D – HRT image with superimposed edges from CFP image, E - fused color CFP image (each band is fused with HRT image), F - fused image (all three bands of CFP image and HRT image are fused into one scalar image) with detected inner and outer optic nerve head contours, G - original HRT image with contours transferred from the fused scalar image.

Due to inaccessibility of golden standard we judge the registration quality subjectively. For this purpose we construct the HRT image with superimposed edges provided by the Canny detector from the green-channel of the CFP. Then we visually compare the correspondence of these CFP edges with the HRT image (fig. 3D). Another type of visual inspection uses image mosaicing (Fig. 3C). According to these auxiliary images we sort images into three groups. In group zero there were only precisely registered images with prefect coincidence of CFP and HRT edges all over the whole image region, in group one there were sufficiently registered with mis-registration in some part of the images smaller than 5 pixels. This mis-registration could be caused by insufficient flexibility of the model of geometric distortion or by finding false local extreme of the similarity criterion. In the third group, there were the mis-registered images with the errors bigger than 5 pixels.

Since the global optimization algorithm is not deterministic, we have made 5 runs over the whole image set to evaluate the stability of the registration. In each of these runs, registered images were sorted into groups and a mark was given for each registered image pair in the following way; for the image from group I the mark was zero, images in the group II have mark one and other images have mark 2. Then average mark was computed for all images. Registration was considered successful when the given image was successfully registered (average mark less or equal one) in all five runs. The results are summarized in the table 1. For further description of the registration algorithm and its testing we refer to [12].

Table 1: Registration results.

Total number of images	334
Group I (precisly registered)	316
Group II (sligthly mis-registered)	13
Group III (mis-registered)	5
Sufficiently registered (I+II)	329
Rate of succes [%]	98.50
Average mark	0.13

After the registration, the image fusion has been made according to the previous chapter. The uncertainty of determination of direction of the maximal amplitude of the change in vector-image was found as the biggest problem of the algorithm. On the fig. 3E, we can see color CFP image with fused details taken from HRT image. For this purpose each band of the color CFP has been fused with HRT image. Our medical colleagues have assessed this color image and considered it very valuable on the other hand it was said that the applicability of this image for the purpose of direct manual segmentation is not as good as the registered CFP-HRT image pair. On the fig. 3F, a scalar image created by fusion of all bands can be seen. The biggest problem of the fusion is that the structure to be detected in the HRT image (optic disc contour) is not exactly the same as in the CFP image (here the outer part of the disc

ISSN: 1727-1983

is much better visible). Therefore, useful but weak information about the correct contour in the HRT image seams to be obscured by the stronger information from the CFP image. However, the automatic method we use for segmenting the optic disc can deal with this fact as it can be seen from the fig. 3F,G. On the other hand, the image fusion provides benefits in some cases, like missing outer ONH contour in HRT and attending outer contour in CFP. For the purpose of segmentation we modified Chrastek's method [8] for the case of fused image. Further experiments are needed to be able to confirm applicability of the algorithm, because the fusion has been tested on a small number of images so far, thus this is open for further research.

Conclusions

We have successfully proposed a new method for registration, fusion and segmentation of ophthalmic images. The method consists of preprocessing step where principle component analysis is done, noise is suppressed by anisotropic diffusion and non-homogenous illumination of both images is corrected. Then we designed a novel registration method making use of robust optimization (controlled random search) of modified mutual information similarity criterion. Quality of the registration step has been evaluated by human observer and reaches 98% of successfully registered images. Further we applied a Scheunder's [4] method for fusion of registered images based on wavelet transform and computation of gradient of vector image. Finally, successful results of segmentation of optic disc contour, done so far on only several images of the test image set, have been presented.

Acknowledgement

Authors sincerely acknowledge the contribution of Prof. G. Michelson, Augen-Klinik Erlangen (Germany) who provided Kowa fundus camera images, data from Heidelberg Retina Tomograph and valuable consultations. Also Radim Chrastek's contribution in optic disc segmentation phase is highly acknowledged. This project has been completed with valuable support by the grant FRVŠ 3118/2005 (Ministry of Education, Czech republic) and also by the support of the research centre DAR , proj. no. ID:1M0572, 1M6798555601.

References

[1] CHAVEZ P.S., KWARTENG A.Y., (1989): 'Extracting spectral contrast in Landsat Thematic Mapper image data using selective principal component analysis', *Photogrammetric Engineering and Remote Sensing*, 55(3), pp. 339-348.

[2] ZHANG Z., BLUM R. S. (1997): 'Multisensor Image Fusion using a Region-Based Wavelet Transform Approach', Proc. of the DARPA IUW, pp. 1447-1451.

[3] Nunez, J., Otazu, X., Fors, O., Prades, A., Pala, V., Arbiol, R. (1999): 'Multiresolution-based image fusion with additive wavelet decomposition'*, IEEE Trans. on Geoscience and Remote Sensing*, Volume: 37 Issue: 3, pp. 1204 -1211

[4] SCHEUNDERS P. (2003): 'An orthogonal wavelet representation of multivalued images', *IEEE Transactions on image processing*, Volume: 12, Issue: 6, pp. 718- 725.

[5] IESTER M., et all. (2001): 'Interobserver variability of optic disk variables measured by confocal scanning laser tomography'. *Am J Ophthalmol.,* 132(1), pp. 57-62

[6] MICHELSON G., GROH M.J. (2001): 'Screening models for glaucoma', *Curr. Opin. Ophthalmol*., 12(2), pp. 105-11.

[7] GREANEY M.J., HOFFMAN D.C., GARWAY-HEATH D.F., NAKLA M., COLEMAN A.L., CAPRIOLI J. (2002): 'Comparison of optic nerve imaging methods to distinguish normal eyes from those with glaucoma', *Invest Ophthalmol Vis Sci*, 43(1), pp. 140-145.

[8] CHRASTEK R., NIEMANNAN H., KUBECKA L., JAN J., DERHARTUNIAN V., MICHELSON G. (2005): 'Optic nerve head segmentation in multimodal retinal images', Proceedings of SPIE Medical Imaging Volume: 5747, pp. 1023-1028

[9] SMITH L. (2002): 'A tutorial on Principal Component Analysis', Internet site adress: http://www.cs.otago.ac.nz/cosc453/student_tutorials/principal_components.pdf

[10] CHRASTEK R, MICHELSON G., DONATH K., WOLF M., AND NIEMANN H. (2000): 'Vessel Segmentation in Retina Scans'. Proc. of 15th Int. EuraSip Conf. EuroConference BIOSIGNAL 2000, Brno, pp. 252–254

[11] PERONA P. AND J. MALIK (1990): 'Scale-space and edge detection using anisotropic diffusion', *IEEE Trans. Pat. Anal.and Machine Int*, 12, pp. 629–639

[12] KUBECKA L., JAN J. (2004): 'Registration of Bimodal Retinal Images - improving modifications' In Proc. 26th Annual Int. Conf. of the IEEE Engineering in Medicine and Biology Society. San Francisco, 2004, pp. 1695 - 1698

[13] MAES F. (1998): 'Segmentation and registration of multimodal medical images', PhD dissert., Kath Univ. Leuven

[14] TSAO J. (2003): 'Interpolation Artifacts in Multimodality Image Registration Based on Maximization of Mutual Information', *IEEE Trans. Med. Imag.*, vol.22, pp.855-864

[15] PLUIM J. P. W., MAINTZ J. B. A., AND VIERGEVER M. A. (2000): 'Interpolation artifacts in mutual information-based image registration', Computer Vision Image Understanding., vol. 77, pp. 211-232

[16] The Heidelberg Retina Tomograph II, Heidelberg Engineering GmbH, Heidelberg, Germany, Internet site: http://www.heidelbergengineering.com

ISSN: 1727-1983